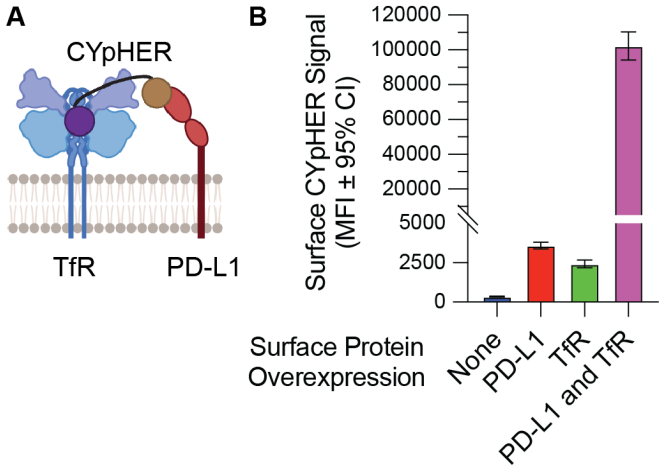


**Supplementary Fig. 1. Prototype PD-L1-binding CYpHER binds both TfR and PD-L1 on cells.** (**A**) Illustration of prototype CYpHER binding both TfR and PD-L1 on a cell surface. (**B**) 293T cells transfected with either TfR-RFP alone ("None" were RFP[-], "TfR" were RFP[+]) or both TfR-RFP and PD-L1-GFP ("PD-L1" were GFP[+]/RFP[-], "PD-L1 and TfR" were GFP[+]/RFP[+]) were incubated with 10 nM 6xHis-tagged prototype PD-L1 CYpHER for 24 hr and then stained with anti-His. Average anti-His signals among cells overexpressing one, the other, both, or neither of TfR and PD-L1 are shown.

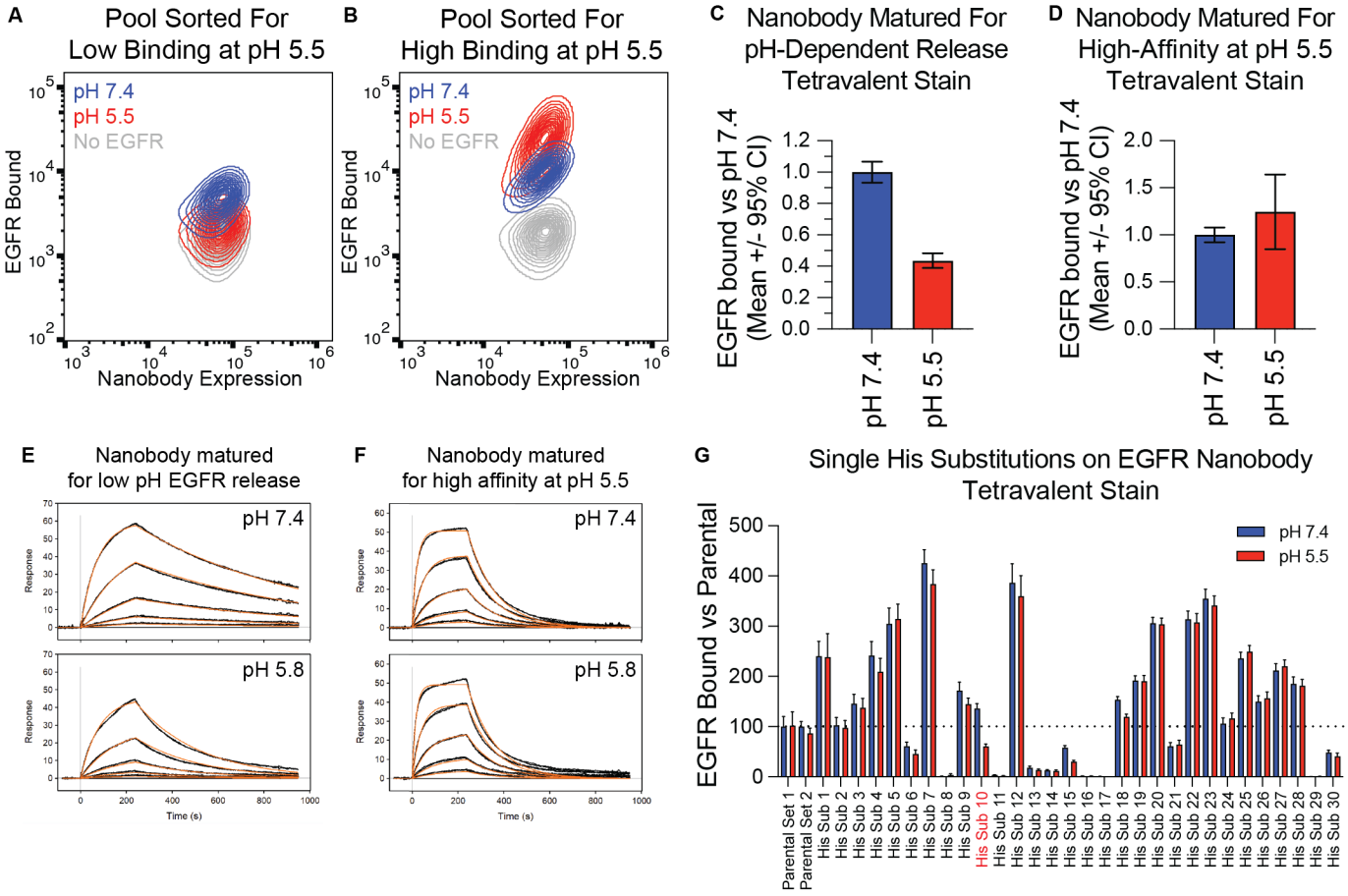


**Supplementary Fig. 2. Engineering an EGFR-binding VHH nanobody for pH-dependent release**. (**A** and **B**) Surface display of nanobody and stain with EGFR followed by rinse at pH 7.4 (high binding, two rounds) or pH 5.5 (low binding, two rounds) enriched for candidates with pH-dependent release. The final round of sorting at pH 5.5 was split into two populations: low binding (**A**), or high binding (**B**). (**C** and **D**) The dominant nanobody variants in the populations from (A) and (B) were stained with biotinylated EGFR and streptavidin followed by pH 7.4 or pH 5.5 rinse. The variant (**C**) from the pH 5.5 low-binding cells (**A**) lost stain in pH 5.5 vs pH 7.4, while the variant (**D**) from the pH 5.5 high-binding cells (**B**) had similar binding in both conditions. (**E** and **F**) Fc fusions of both nanobody variants were tested in surface plasmon resonance for EGFR binding in pH 7.4 (top) or pH 5.8 (bottom) buffers. (**G**) EGFR-binding VHH nanobody was subjected to conventional Histidine scanning, and singleton variants analyzed for binding to biotinylated EGFR + streptavidin followed by pH 7.4 or pH 5.5 rinse. His substitution 10 had the greatest difference in staining and was selected.

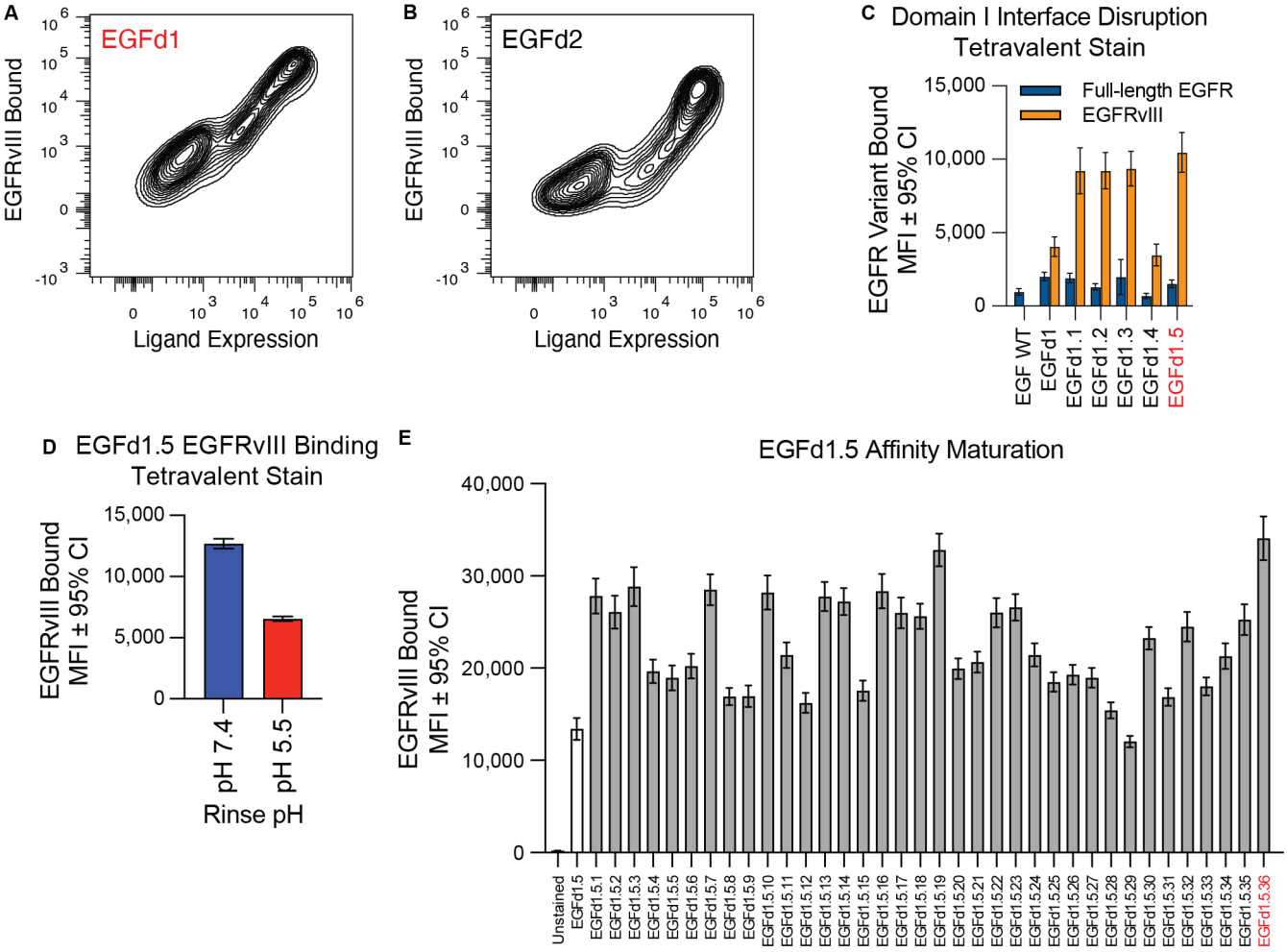


**Supplementary Fig. 3. Adapting EGF for use in CYpHER.** (**A** and **B**) Rosetta protein design was used with an EGF and EGFR co-crystal structure (PDB 1IVO) to design variants with improved predicted binding strength to Domain III. 1000 such variants were displayed on 293F cells and stained with biotinylated EGFRvIII and fluorescent streptavidin. After three rounds of sorting and enrichment for high-staining cells, singleton candidates were tested for EGFRvIII binding, two of which validated. One (EGFd1) was advanced. (**C**) The interface between EGF and EGFR Domain I was studied, identifying four residues predicted to be key to the interaction. These were mutated to disrupt the interaction, as singletons (EGFd1.1 to EGFd1.4) or all four at once (EGFd1.5). These were surface displayed on 293F cells and stained with biotinylated EGFR (full length) or EGFRvIII and fluorescent streptavidin. EGFd1.5 (highest staining with EGFRvIII, low binding to full length EGFR) was advanced. (**D**) EGFd1.5 was tested in surface display for biotinylated EGFRvIII + fluorescent streptavidin binding followed by pH 7.4 or pH 5.5 rinse. (**E**) Two rounds of site-saturation mutagenesis affinity maturation of EGFd1.5, followed by combining enriched mutations into 36 variant candidates, yielded binders with improved EGFRvIII binding. EGFd1.5.36 was selected.

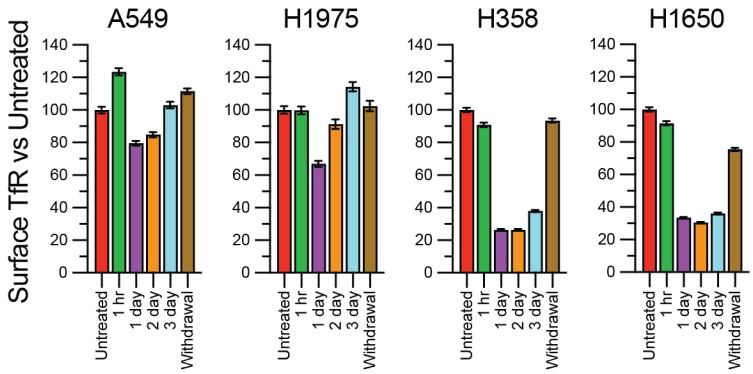


**Supplementary Fig. 4. CYpHER effect on surface TfR levels in cancer cell lines.** A549, H1975, H358, and H1650 cells untreated or treated with 10 nM CT-1212-1 for 1 hr, 1 day, 2 days, 3 days, or 1 day followed by 1 day without drug ("Withdrawal") and then analyzed by flow cytometry for surface TfR levels.

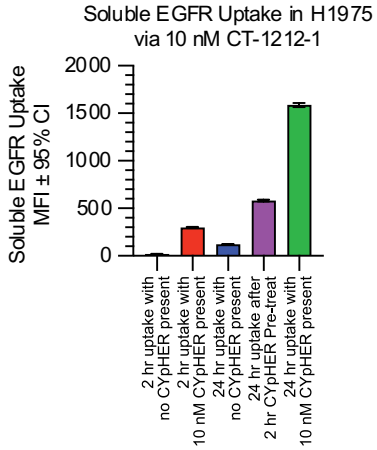


**Supplementary Fig. 5. Soluble EGFR uptake with or without CYpHER withdrawal**. Soluble EGFR uptake after: 2 hr with 10 nM fluorescent soluble EGFR but no CYpHER (bar 1); 2 hr with 5 nM CT-1212-1 saturated with fluorescent soluble EGFR (bar 2); 24 hr with 10 nM fluorescent soluble EGFR but no CYpHER (bar 3); 24 hr incubation with 10 nM fluorescent soluble EGFR (but no CYpHER) after 2 hr pre-treatment with 5 nM CT-1212-1 saturated with unlabeled EGFR (bar 4); or 24 hr with 5 nM CT-1212-1 saturated with fluorescent soluble EGFR (bar 5).

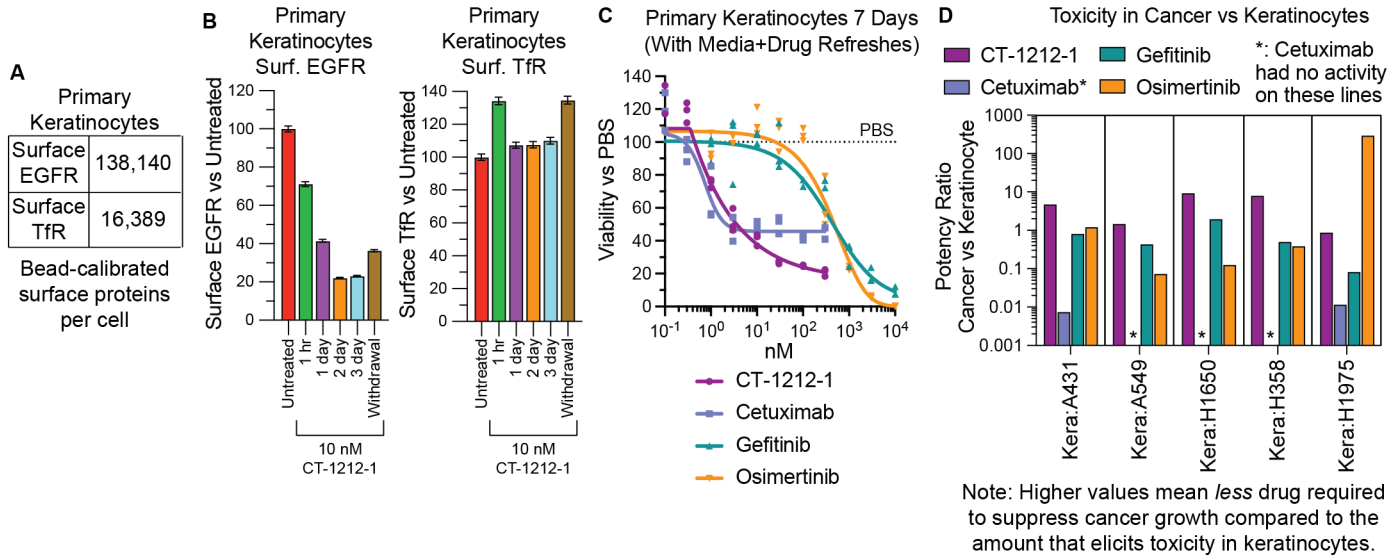


**Supplementary Fig. 6. Effect of CYpHER on primary keratinocytes.** (**A**) Primary human dermal keratinocytes were flow analyzed alongside calibration beads to quantitate surface EGFR and TfR levels. (**B**) Keratinocytes were untreated or treated with 10 nM CT-1212-1 for 1 hr, 1 day, 2 days, 3 days, or 1 day followed by 1 day without drug ("Withdrawal") and then analyzed by flow cytometry for surface EGFR levels (left) and surface TfR levels (right). (**C**) Keratinocytes were treated for 7 days, with a media exchange (including drug refresh) on day 4, with CT-1212-1, cetuximab, gefitinib, or osimertinib. After treatment, cell levels per well were quantitated by CellTiter-Glo 2.0 assay. (**D**) EC50 values of cancer cell lines (Fig. 7I) compared to the EC50 values (asymmetric sigmoidal [5PL] curve fit) of the primary keratinocyte treatments. Ratio with keratinocyte EC50 as numerator and cancer line EC50 as denominator results in higher values when compound is more potent at suppressing growth of cancer lines relative to effect on keratinocyte growth.

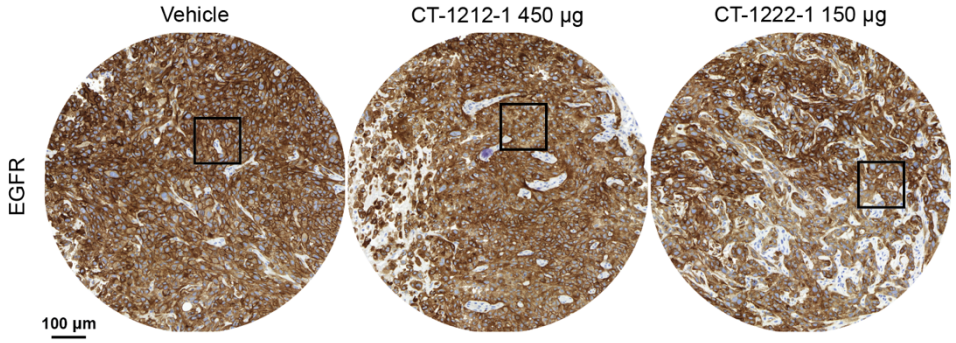


**Supplementary Fig. 7. Full fields of EGFR histology shown cropped in Fig. 8F.** The bounding boxes identify the crop areas used in Fig. 8F.